EUROPEAN ORGANIZATION FOR NUCLEAR RESEARCH
CERN - ACCELERATORS AND TECHNOLOGY SECTOR

**CERN-ATS-2013-046**

# Thermo-electric Analysis of the Interconnection of the LHC main Superconducting Bus Bars

P.P. Granieri[a,b], M. Breschi[c], M. Casali[c], L. Bottura[a], A. Siemko[a]
a TE Department, CERN, Geneva, Switzerland
b Swiss Federal Institute of Technology (EPFL), Particle Accelerator Physics Laboratory (LPAP), Lausanne, Switzerland
c University of Bologna, Department of Electrical Engineering (DIE), Italy

Spurred by the question of the maximum allowable energy for the operation of the Large Hadron Collider (LHC), we have progressed in the understanding of the thermo-electric behavior of the 13 kA superconducting bus bars interconnecting its main magnets. A deep insight of the underlying mechanisms is required to ensure the protection of the accelerator against undesired effects of resistive transitions. This is especially important in case of defective interconnections which can jeopardize the operation of the whole LHC.

In this paper we present a numerical model of the interconnections between the main dipole and quadrupole magnets, validated against experimental tests of an interconnection sample with a purposely built-in defect. We consider defective interconnections featuring a lack of bonding among the superconducting cables and the copper stabilizer components, such as those that could be present in the machine. We evaluate the critical defect length limiting the maximum allowable current for powering the magnets. We determine the dependence of the critical defect length on different parameters as the heat transfer towards the cooling helium bath, the quality of manufacturing, the operating conditions and the protection system parameters, and discuss the relevant mechanisms.



Published in "Cryogenics", 53 (2013) 107-118

Geneva, Switzerland

July 2013

Cryogenics 53 (2013) 107–118

Contents lists available at SciVerse ScienceDirect

Cryogenics

journal homepage: www.elsevier.com/locate/cryogenics

# Thermo-electric analysis of the interconnection of the LHC main superconducting bus bars

P.P. Granieri [a,b,*], M. Breschi [c], M. Casali [c], L. Bottura [a], A. Siemko [a]

[a] TE Department, CERN, Geneva, Switzerland
[b] Swiss Federal Institute of Technology (EPFL), Particle Accelerator Physics Laboratory (LPAP), Lausanne, Switzerland
[c] University of Bologna, Department of Electrical Engineering (DIE), Italy

ARTICLE INFO

*Article history:*
Available online 17 June 2012

*Keywords:*
Accelerator magnets
Interconnections
LHC
Superconducting bus bar

ABSTRACT

Spurred by the question of the maximum allowable energy for the operation of the Large Hadron Collider (LHC), we have progressed in the understanding of the thermo-electric behavior of the 13 kA superconducting bus bars interconnecting its main magnets. A deep insight of the underlying mechanisms is required to ensure the protection of the accelerator against undesired effects of resistive transitions. This is especially important in case of defective interconnections which can jeopardize the operation of the whole LHC.

In this paper we present a numerical model of the interconnections between the main dipole and quadrupole magnets, validated against experimental tests of an interconnection sample with a purposely built-in defect. We consider defective interconnections featuring a lack of bonding among the superconducting cables and the copper stabilizer components, such as those that could be present in the machine. We evaluate the critical defect length limiting the maximum allowable current for powering the magnets. We determine the dependence of the critical defect length on different parameters as the heat transfer towards the cooling helium bath, the quality of manufacturing, the operating conditions and the protection system parameters, and discuss the relevant mechanisms.



## 1. Introduction

A few days after its start-up in September 2008, the particle accelerator Large Hadron Collider (LHC) at CERN experienced an incident causing considerable damages and delaying the restart of the machine by more than 1 year. The incident was initiated by an electrical fault due to a defective interconnection (IC) between two adjacent main dipole magnets [1,2]. The fault consisted of a bad soldering between the two superconducting (SC) cables in the bus bar and between the cables and the copper stabilizer, along with a lack of longitudinal continuity in the stabilizer, whose role is to guarantee the protection of the circuit. Furthermore, the sensitivity of the bus bar quench detection system was not sufficient to detect the voltage rise of the resistive zone, because the intervention threshold was set too high.

Large efforts were undertaken to measure the resistance of the interconnections in the machine both at warm and at cold [3]. They included a calorimetric technique and electrical measurements performed using either invasive or non-invasive diagnostics. The invasive technique requires direct access to a single interconnection: it consists of room temperature electrical resistance measurement allowing to quantify the longitudinal continuity of the copper stabilizer across it. The non-invasive electrical resistance measurements were carried out at room and cryogenic temperatures exploiting the magnet voltage taps. They covered therefore a bus bar segment containing more than one interconnection, and the interpretation depended on the Residual Resistivity Ratio (*RRR*) of the copper bus bar. Furthermore, gamma-radiography was used to visualize the internal volume of the interconnections. This measurements campaign allowed determining the presence of defects in the machine, as well as their dimension. The largest defects were repaired [4] before the LHC restart in November 2009. However, a number of low quality interconnections could still be present in the accelerator. For this reason the decision was taken to limit the maximum current in the main circuits, until the full consolidation campaign [5] that will take place in 2013–2014. A new quench detection system across the interconnections is implemented with a reduced sensitivity threshold, as well as other remedies [2].

In this paper we present a numerical thermo-electrical model of the LHC superconducting bus bars and interconnections, both for the Main Bending (MB) dipole and Main Quadrupole (MQ) magnets. The model aims at estimating the critical length of the interconnection defect. It is validated by reproducing experimental tests of a defective interconnection sample. We report investiga-

* Corresponding author at: TE Department, CERN, Geneva, Switzerland. Tel.: +41 227676277.
*E-mail address:* pier.paolo.granieri@cern.ch (P.P. Granieri).

0011-2275/$ - see front matter © 2012 Elsevier Ltd. All rights reserved.
http://dx.doi.org/10.1016/j.cryogenics.2012.05.009

tions of the heat transfer towards the cooling helium bath in the interconnection and bus bar region, and evaluate its impact on the calculations. The influence of the quality of manufacturing, operating conditions and protection system parameters is analyzed as well. Parametric analyses are presented, in adiabatic and non-adiabatic conditions, as a function of the defect dimension, current decay time constant, *RRR* of the copper of the SC cable matrix and of the stabilizer, spatial distribution of the defect.

## 2. The LHC main superconducting bus bars and interconnections

The 13 kA bus bar connecting the LHC MB dipole and MQ magnets is made of type 02 [6] superconducting cable embedded in a hollow copper stabilizer piece [7]. The cable can be seen in the left and right extremities of Fig. 1, where the copper stabilizer is cut to show the bus bar cross-section. The void space inside the stabilizer must be filled with tin–silver alloy to provide good thermal and electrical contact between the bus bar constituents.

As soon as a quench is detected in a magnet, its coil is immediately heated and electrically by-passed by means of a cold diode, so that the coil current decays to almost zero in less than 1 s. Meanwhile the bus bar by-passing the quenched magnet, as well as the other magnets of the sector, all powered in series, still carry the full current which is decaying almost exponentially with a time constant of tens of seconds [8]. The bus bar was therefore designed with a copper cross-section sufficient to safely carry the current during discharge, in case its superconducting cable undergoes a resistive transition. The design of the MB and MQ bus bars is identical except for the copper cross-section [7] that is larger in case of the MB bus bars because of the larger current decay time constant (initial time constant of around 104 s for MB vs. 37 s for MQ at the nominal beam energy of 7 TeV).

The exploded view of the bus bar interconnection between two adjacent MB or MQ magnets is schematically shown in Fig. 1. It is composed of a 120 mm long flat and a 150 mm long U-shaped copper profile that enclose the 120 mm long overlapping zone of the two superconducting cables coming from the right and left side magnets. A soft soldering technique [9] based on tin–silver alloy is used to splice the superconducting cables between them and to the interconnection stabilizer, as well as to connect the interconnection stabilizer to the bus bar copper profile. A well soldered interconnection, where all the void inner spaces are filled with solder, looks like a continuation of the bus bar as shown in Fig. 2. This ensures a good thermal and electrical coupling between all the interconnection constituents both in superconducting and resistive state. The stabilizer should hence work as a continuous electrical shunt for the cable.

The bus bar is electrically insulated by means of polyimide and ISOPREG EP2047 tapes [7], whereas the interconnection insulation is made of ~200 mm long U-shaped polyimide and VP-310 pieces

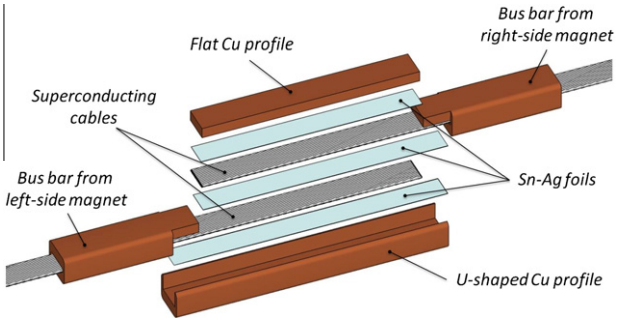


**Fig. 1.** View of the bus bar interconnection constituents.

[10]. The bus bar is inserted in a horizontal pipe and cooled by static pressurized He II at 1.9 K.

In order to limit the heat dissipation in the interconnection due to Joule effect, the electric resistance between superconducting cables is specified to be lower than 0.6 nΩ [9]. The measured resistances on samples during production were below this design value. However, the calorimetric technique developed after September 2008 allowed determining the actual electric resistance associated to the measured temperature increase, corresponding to a value between 180 and 260 nΩ for the interconnection initiating the incident [2]. This high value was identified as the cause of the quench. Note that a resistive transition of a bus bar interconnection can also be induced by external heating, for instance due to warm helium coming from a nearby quenching magnet.

A bus bar quench is not a fault condition, given the presence of a large copper stabilizer cross-section. However, it can trigger a thermal runaway in case of the concurrent presence of two manufacturing defects [11,12]: lack of transverse contact between cable and copper stabilizer (Fig. 3) and lack of longitudinal continuity in the copper stabilizer. The scheme of a defective interconnection featuring such defects is shown in Fig. 4. The combination of the two defects prevents current redistribution between cable and stabilizer: the total operating current is forced to flow through the superconducting cable along the defect length, which is the bus bar length where at least one of the two defects is present. The interconnection can therefore experience a thermal runaway, depending on the length of the defect zone. This length determines whether or not the dissipation by Joule heating is balanced by the heat evacuated towards the coolant and by longitudinal solid conduction through the bus bar.

## 3. Model

### 3.1. Description

The multi-physics model adopted for the analysis is the CryoSoft code THEA, described in detail in [13], that allows taking into account the material properties dependence on temperature, current and magnetic field. THEA is based on the assumption that the components length is much larger than their transverse dimension, so that all phenomena can be analyzed with a 1-D approximation. However, considerable efforts are made for the definition of the transverse heat transfer towards the cooling bath. The longitudinal length is discretized with a non-uniform mesh in the frame of a finite element approach.

The bus bar is modeled as a single homogeneous thermal element with uniform temperature over the cross-section. The total cross-section $A_b$ of the bus bar (subscript $b$) is obtained as sum of the partial cross-sections of the constituents, i.e. the superconducting filaments, the copper stabilizer matrix of the strands and, when present, the copper stabilizer of the bus bar. The homogenized density $\rho_b$ and thermal conductivity $k_b$ are obtained weighting on the area, whereas the homogenized specific heat $C_b$ is obtained weighting on the mass of the constituents. The bus bar thermal capacity, the heat transport by conduction, the heat exchange at the interface with the cooling medium and the Joule heat generation $\dot{q}'_{Joule,b}$ are described by the following thermal equation:

$$A_b\rho_b C_b\frac{\partial T_b}{\partial t}-\frac{\partial}{\partial x}\left(A_b k_b\frac{\partial T_b}{\partial x}\right)+p_{b\_He}HTC(T_b-T_{He})=\dot{q}'_{Joule,b}. \quad (1)$$

$T_b$ and $T_{He}$ are the bus bar and helium temperature, $p_{b\_He}$ and $HTC$ represent the wetted perimeter and the heat transfer coefficient, respectively. The temperature of the helium hydraulic component $T_{He}$ is calculated by the equations that model compressible flow in a 1-D pipe, detailed in [13], that complement Eq. (1). Considering

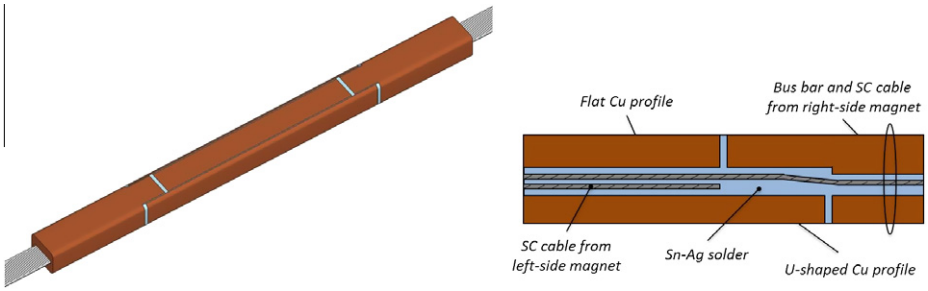


**Fig. 2.** Left: 3-D sketch of a well soldered interconnection. Right: longitudinal cross-section of its right-hand side.

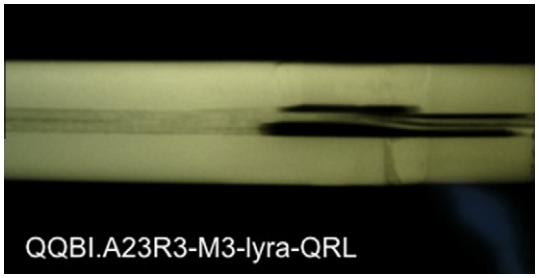


**Fig. 3.** γ-Ray picture of the right-side of a defective interconnection [1].

all the bus bar components lumped into a unique element does not allow catching the details of the current distribution phenomena, which would require the definition of the cable and bus bar as separate thermal and electrical elements. On the other hand, the one element approach was demonstrated to be appropriate when considering heating sources distributed across the whole cross-section [14].

The concurrent presence of transverse and longitudinal lack of solder in the interconnection, as described in the previous section, is considered in the calculations. This makes the model more complete than previous studies that had taken into account either a local resistive heating due to faulty splices assuming a longitudinal continuity of the bus bar stabilizer [15], or the only reduction of the stabilizer cross-section in the longitudinal direction. The complex geometry of a defective interconnection is simulated by the absence of copper stabilizer over a length where at least one of the two defects is present, as shown in Fig. 5. This is the region where the total current has to flow through the superconducting cable. The two pieces of the copper stabilizer that are not in contact with the cable are not taken into account, as they behave like open circuits from the electrical standpoint. This geometrical approximation underestimates the copper heat capacity. On the other hand it makes the investigated domain symmetric, thus allowing halving it (as shown in Fig. 5c) and saving a considerable amount of computation time.

It is worth noticing that the defect length $L_d$ is directly proportional to $R_{add}$, the additional resistance with respect to the nominal value of a good interconnection at room temperature. Typical resistances of good interconnections are 10–12 μΩ for MB and 17-19 μΩ for MQ [4,16]. $R_{add}$ can be determined through room temperature electrical measurements. Once $L_d$ is calculated through the model, it can be converted into the equivalent $R_{add}$ using for instance the following formula:

$$R_{add} = \frac{\rho_{el}}{n_{st} \cdot A_{st} \cdot A_{Cu}/(A_{Cu} + A_{SC})} \cdot L_d. \quad (2)$$

$\rho_{el}$ is the resistivity of the SC cable copper matrix at room temperature, $n_{st}$ is the number of strands in the cable, $A_{st}$ is the strand cross section and $A_{Cu}$ and $A_{SC}$ are the strand copper and superconducting area, respectively.

### 3.2. Implementation

As previously stated, the manufacturing imperfections can be dangerous in case of a resistive transition of the bus bar. As long as the cable is in the superconducting state the transport current flows in the Nb–Ti filaments without heat dissipation, except for the dissipation due to the inter-cables contact resistance. As soon as a quench occurs the current starts flowing from the superconducting filaments to the strand copper matrix, then possibly to the bus bar copper stabilizer. The parametric studies presented consider a quench already developed over the sample: an initial temperature of 10 K is assumed, slightly above the critical temperature $T_c$ of 9.01 K. Besides the Joule heating, there are no other heating sources. The assumption of adiabatic boundary conditions is made, for every transversal heat transfer model considered. However, it was assessed that the boundary conditions have a negligible impact on the calculations.

The numerical analysis aims at finding the minimum defect length leading to a thermal runaway. The criterion taken is a hot spot temperature in excess of the melting of SnAg and polyimide

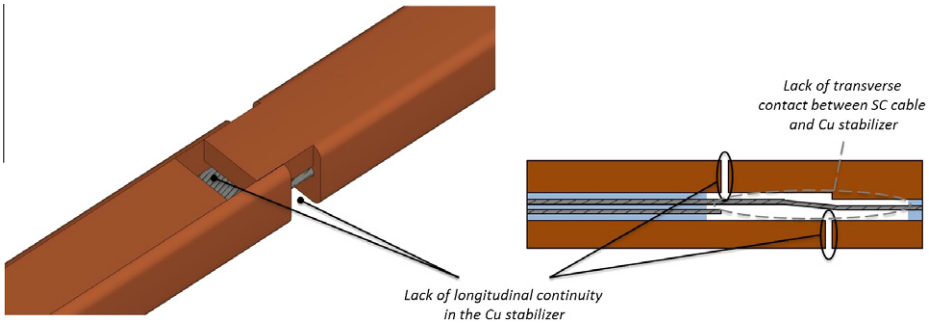


**Fig. 4.** 3-D view (left) and longitudinal cross-section (right) of one side of a defective interconnection. The two kinds of defect are highlighted.

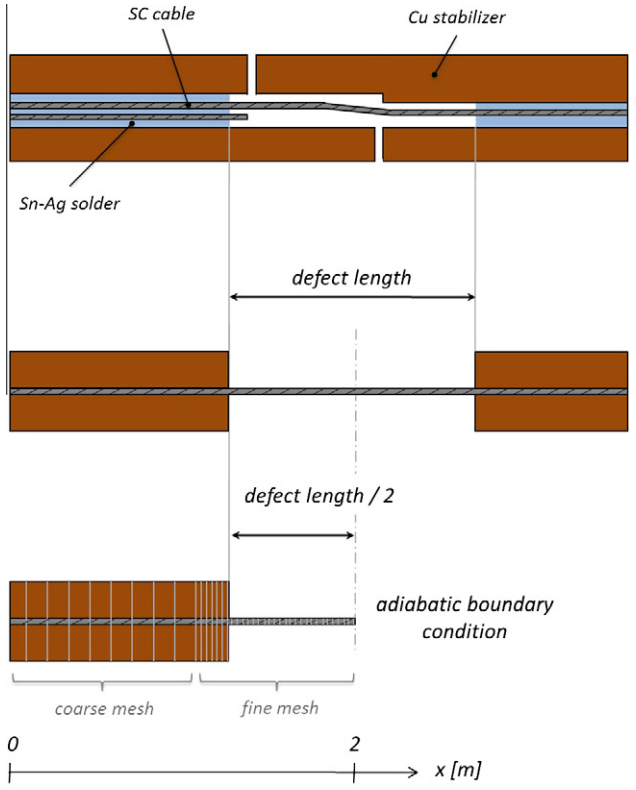


**Fig. 5.** From top to bottom: scheme of an interconnection with a single defect; modeling concept; model with half the defect length assumed for the calculations. Not to scale.

of the interconnection, assumed to occur at 500 K. A trial length is selected and the transient temperature profile is observed. The defect length is then adjusted according to the maximum temperature reached, and a new transient is simulated. This trial-and-error procedure is repeated until the difference between the largest defect leading to a controlled quench and the smallest defect leading to a thermal runaway is equal to 1 mm.

In all simulations with a single defect a 2 m long sample is considered (with half the defect length), whereas a 4 m long sample is considered for the case of double defects (total defect length). The bus bar cross section, and consequently its properties, is a function of position. The Nb–Ti cross-section is constant all over the sample because the presence of one single superconducting cable is considered. The copper cross-section is equal to the sum of the copper stabilizer of the superconducting cable and of that of the bus bar outside the defect, whereas it is equal to the only copper of the superconducting cable in the defect. Since the *RRR* of the two types of copper differ because of different manufacturing processes, the value considered in the calculations is the average *RRR* weighted on the area outside the defect, or the *RRR* of the SC cable copper inside it. Because of the uncertainty of the *RRR* values of the accelerator components [17], a parametric study is performed and shown in next section: the cable *RRR* is varied between 80 and 160, whereas the bus bar *RRR* is varied between 100 and 220. Default values are set to the conservative 80 and 100, respectively. The SnAg solder is not considered to avoid unnecessary complication of the model. The polyimide electrical insulation is not defined as an additional thermal component. Its presence is taken into account in the definition of the heat transfer coefficient to helium, as reported in Section 3.3. The geometric parameters considered for calculations are reported in Table 1.

The transport current is varied between 3 and 13 kA, corresponding to beam energies between 1.8 and 7.7 TeV, respectively. The bus bar is subjected to its magnetic self-field, ranging between 0.12 and 0.52 T depending on the current. The current is kept constant until the detection time $\tau_{det}$ is reached. Then it decays exponentially with the time constant $\tau_{dump}$. The detection time was determined calculating the voltage developed per meter of MB bus bar from the copper resistivity at room temperature $\rho_{el}$, the $RRR_{bus}$ here assumed to be 215 [7], the bus bar copper cross-section $A_{Cu}$ and the current $I$. Considering a voltage threshold $V_{th}$ of 0.3 mV at 7 TeV of the new quench detection system [2] and the measured quench propagation velocity $v_q$ = 0.4 m/s [18], $\tau_{det}$ for $I$ = 13 kA can be calculated as:

$$\tau_{\mathrm{det}} = \frac{V_{th}}{v_q \cdot \left(\frac{\rho_{el} \cdot I}{RRR_{bus} \cdot A_{Cu}}\right)} = 0.2\ \mathrm{s}. \tag{3}$$

For simplicity and in order not to affect the parametric studies, the same detection time is considered for the MB and MQ bus bar, for any current. The time constant of the current decay depends on the set-up of the dumping resistor in parallel to the magnets circuit that is activated in case of a magnet quench, as well as on the current (or beam energy) level. The $\tau_{dump}$ is varied in our simulations to perform the parametric analyses reported in Section 5. Unless specified otherwise, its value is taken equal to 100 and 20 s for the MB and MQ circuit, respectively.

The bus bar is in contact through the electrical insulation with the static He II coolant filling the pipe. No helium is assumed to be inside the bus bar or inside the interconnection. The considered operating conditions of 1.9 K and 0.1 MPa are imposed as initial conditions, as well as boundary conditions for the coolant. In order to assess the impact of the cooling, other heat transfer modes are also considered, namely He I and the adiabatic case. The heat transfer coefficients $HTC_s$ are detailed in Section 3.3. The operating parameters used for the calculations are reported in Table 2.

As far as the simulation parameters are concerned, convergence studies were performed to obtain confidence in the results and set appropriate values of the space and time step to be used for the numerical integration. Calculations were repeated varying the number of elements in the mesh as well as the time step. As for the mesh, if on the one hand the system sensitivity to the defect length requires short elements, on the other hand a minimum length of the bus bar is needed to avoid that the boundary conditions affect the results. Fulfilling both requirements using a uniform mesh would result in a very large number of elements (at least 0.5 mm long elements over a 2 m long bus bar, thus 4000 elements), meaning long computation times. A static optimized mesh was therefore developed, subdividing the physical domain into two different parts as shown in Fig. 5c:

- a *fine mesh* in the interconnection region, including the defect;
- a *coarse mesh* zone at the edge, far from the defect zone.

The convergence studies, carried out for different defect lengths, investigated the element size inside the fine zone and inside the coarse zone, as well as the length of the fine zone. They showed that, for defects smaller than 3 cm, the elements length in the defect region should be smaller than 0.5 mm to catch the solution features. For defects larger than 3 cm, a uniform mesh with 2.5 mm long elements is sufficient for the scope of the analyses and does not require long computation times. As for the time step, the convergence study indicated that time steps shorter than 10 ms at the beginning of the transient and limited to a maximum of 0.1 s are suitable.

### 3.3. Heat transfer to the helium cooling bath

The mechanisms of heat transfer from bus bar and interconnection towards the helium bath are of crucial importance for the modeling, as it will be shown. A dedicated test provided the heat

**Table 1**
Geometric parameters of the MB and MQ bus bar considered for the calculations.

| | | MB | MQ |
|---|---|---|---|
| Sample length | (m) | 2 | |
| SC strand | | | |
| Strand diameter | (mm) | 0.825 | |
| Cu to Nb–Ti ratio | (-) | 1.95 | |
| SC cable | | | |
| Number of strands | (-) | 36 | |
| Thin edge thickness | (mm) | 1.362 | |
| Thick edge thickness | (mm) | 1.598 | |
| Width | (mm) | 15.1 | |
| Bus bar | | | |
| Internal dimensions | (mm × mm) | 16 × 3 | |
| External dimensions | (mm × mm) | 20 × 16 | 20 × 10 |
| Cable *RRR* range | (-) | 80–160 | |
| Bus bar *RRR* range | (-) | 100–220 | |
| Cross-sections | | | |
| Nb–Ti | ($mm^2$) | 6.523 | |
| SC cable Cu stabilizer | ($mm^2$) | 12.72 | |
| Bus Bar Cu stabilizer | ($mm^2$) | 266.64 | 146.64 |
| He | ($mm^2$) | 4353 | 4593 |
| Wetted perimeter | (mm) | 74.4 | 62.4 |
| He hydraulic diameter | (mm) | 69.29 | 73.11 |

**Table 2**
Operating parameters of the MB and MQ bus bar considered for the calculations.

| | | MB | MQ |
|---|---|---|---|
| Nominal current | (kA) | 11.85 | |
| Nominal beam energy | (TeV) | 7 | |
| Current range | (kA) | 3–13 | |
| Beam energy range | (TeV) | 1.8–7.7 | |
| Nominal magnetic self-field | (T) | 0.47 | |
| Magnetic self-field range | (T) | 0.12–0.52 | |
| Detection time $\tau_{det}$ | (s) | 0.2 | |
| Nominal decay time constant $\tau_{dump}$ | (s) | 100 | 20 |
| $\tau_{dump}$ range | (s) | 50–100 | 10–30 |
| Initial Bus Bar temperature | (K) | 10 | |
| SC cable critical temperature $T_c$ | (K) | 9.01 | |
| Nominal He initial temperature $T_{He\ in}$ | (K) | 1.9 | |
| $T_{He\ in}$ range | (K) | 1.9–4.25 | |
| He initial pressure $P_{He\ in}$ | (MPa) | 0.1 | |
| He mass flow | (g/s) | 0 | |
| Bus bar boundary conditions | | Adiabatic | |
| He boundary conditions | | $T = T_{He\ in}$, $P = P_{He\ in}$ | |

transfer coefficient through the bus bar electrical insulation ($HTC_{bus}$) in He II and He I bath for a limited range of temperatures. The data analysis allowed extending the results to higher temperatures. The results of this study, which can be found in [19], are summarized in Fig. 6. The HTC features larger values in He I than in He II bath, because the dominant heat extraction mechanism is thermal conduction through the polyimide insulation. In these experimental and theoretical studies, a constant bath temperature was considered. However, the validity of such hypothesis has not been demonstrated in the LHC conditions. In a first approximation of heat deposit localized in the middle of the defect and assuming turbulent He II heat transport law, an axial cooling power of around 100 W would be provided along the sample, while maintaining the superfluid helium state. This would allow extracting the heat deposited in an interconnection experiencing a runaway in nominal operating conditions, and maintaining the mentioned HTC. In case of He I bath, the latent heat of the helium volume surrounding the bus bar would be greater than the heat deposited for the typical duration of a controlled quench or runaway. That would result also in this case in a constant bath temperature.

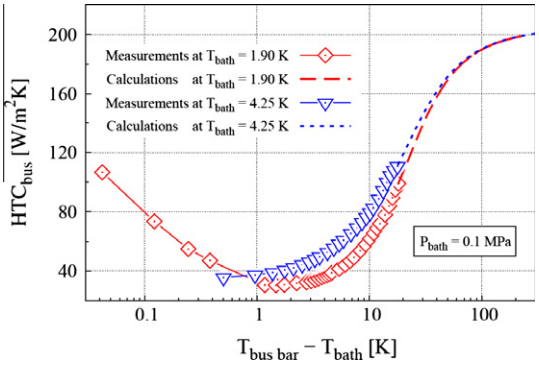


**Fig. 6.** Measured and calculated bus bar heat transfer coefficient as a function of the temperature difference, for bath temperature of 1.9 and 4.25 K.

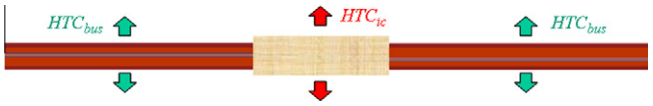


**Fig. 7.** Sketch of the bus bar and interconnection heat transfer coefficients: $HTC_{bus}$ and $HTC_{ic}$.

While a good knowledge of the heat transfer coefficient through the bus bar insulation ($HTC_{bus}$) was obtained, a complete description of the heat transfer coefficient through the interconnection insulation ($HTC_{ic}$) would require further investigations. Fig. 7 schematically shows the regions of the two heat transfer coefficients. $HTC_{ic}$ can be derived from the investigation of experimental tests reproducing defective interconnections [20], thus allowing further improving the reliability of the calculations. An analysis based on local heat transfer coefficients has provided information in this direction [21] and the main results are summarized in the next section. For the parametric analyses reported in Section 5, two different approaches are considered: either the same bus bar heat transfer coefficient is assumed everywhere, that is $HTC_{ic} = HTC_{bus}$, or the conservative assumption of an adiabatic interconnection is made ($HTC_{ic} = 0$). In the first case, the bus bar wetted perimeter is assumed over the whole sample length. Unless specified otherwise, the cooling bath is considered at the nominal temperature of 1.9 K.

## 4. Model validation

Prior to the presentation of the parametric analyses, we report in this section the validation of the model, which was performed by simulating experimental tests of an interconnection sample featuring a purposely built-in defect. The setup details and experimental results are described in [20]. The analyses here reported refer to tests in He I bath without external magnetic field. The considered instrumented sample features a 35 mm long defect located on one side of the interconnection, corresponding to an additional resistance $R_{add}$ of 42 μΩ. Fig. 8 shows a sketch of the sample longitudinal cross-section, where the defect is created by polyimide layers around the superconducting cables and between interconnection and bus bar stabilizer. Thermofoil heaters are placed in contact with the interconnection (heater *W*) and the bus bar stabilizer (heater *M*) to start the normal zone. The thermo-couple junctions *P*2, *U* and *M*1 are located inside the left bus bar, interconnection and right bus bar Cu stabilizer, respectively.

The modeling approach presented in the previous section is used, accounting in this case also for the details of the interconnection region and focusing on the definition of local heat transfer

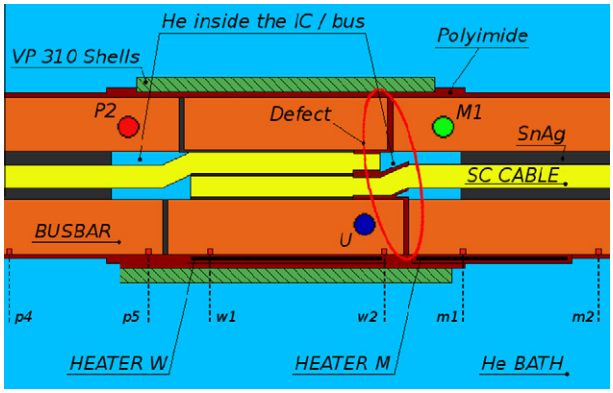


**Fig. 8.** Sketch of the longitudinal cross-section of the tested sample (side view).

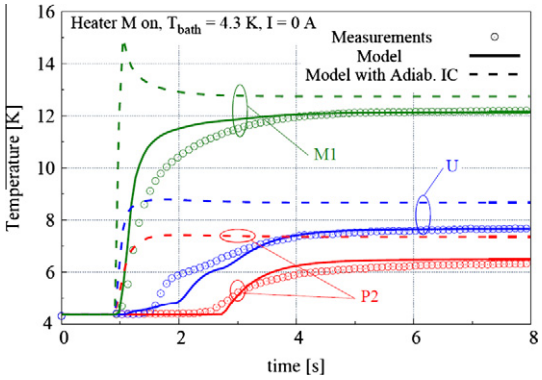


**Fig. 9.** Measured vs. calculated temperatures in case of no current and only heater *M* switched on.

coefficients. The extensive description of the model and of the results is reported elsewhere [21]. In particular, the superconducting cables and the Cu stabilizer are defined as separate thermal and electric elements, whereas the heaters constitute the third thermal element. The thermal resistances among the elements are defined by solid conduction through polyimide and SnAg layers. The heat transfer coefficient between the Cu stabilizer and the bath in the bus bar region is the one reported in Fig. 6. For the interconnection region, the heat transfer coefficient is given by solid conduction through the polyimide and fiberglass layers, whether the stabilizer temperature is below 6.5 K. The fiberglass is used to model the VP310 material. Above 6.5 K the thermally insulating film boiling layer is considered, described by a heat transfer coefficient of 250 W/m$^2$ K. The threshold temperature represents a rough model to describe film boiling formation in the interconnection. It is calculated from the heat flux at which, according to [19], film boiling formation is estimated to occur around the bus bar. As for the heat transfer from stabilizer and cables to the He filling the void spaces inside interconnection and bus bar, it is described by the Kapitza resistance Cu–He before the He vaporizes and by the film boiling heat transfer coefficient afterwards. The geometric and operating parameters are set equal to the measured values.

Fig. 9 reports measured and calculated temperatures for a heater calibration test: only heater *M* was turned on for 30 s with a power of 18 W, without any current flowing in the sample. The steady-state temperature, reached after few seconds, is higher for the sensor located below the heater *M* than for the sensors on the other side of the defect.

The calculations are performed using both a simplified model featuring an adiabatic interconnection and the above mentioned complete model. The first model, assuming no heat transfer towards the He bath and no He filling the void spaces inside interconnection and bus bar, does not catch the features of the measurements. The calculated steady-state temperatures are higher than the measured ones, the transient states are also very different and the measured time delays are not predicted. The complete model instead well simulates the test. The heat transfer through the interconnection insulation lowers the steady-state temperatures that are correct within 0.2 K. The He inside the interconnection and the bus bar allows reproducing the transient features and the initial time delays. It is worth noticing that the changes of slope of the calculated curves, which reflect those of the measured ones, are associated to boiling of the He inside interconnection and bus bar. In particular the first change of slope of the calculated *U* curve occurring at 2 s is associated to the end of boiling of the He close to the defect. The second change of slope at 2.4 s corresponds to the start of boiling of the He located at the left interconnection extremity. The end of boiling of this He occurs at 2.7 s when the *U* curve features the last change of slope and the *P*2 sensor, located just on top of this He, starts heating up.

In the tests with current the heat sources are both external and internal, respectively due to heaters *M* and *W* both turned on and to Joule heating in the resistive components. Fig. 10 reports the time evolution of the three thermo-couple junctions. The current is ramped up to the constant level of 11 kA and no temperature increase or voltage is detected in the first second, before the heaters are fired. The heat pulses of 15 W for heater *M* and 14 W for heater *W* last between 1 and 2.2 s. Due to larger heat generation and less efficient heat extraction, the temperature increase in the defect zone is larger than in the left side of the interconnection. As soon as the voltage threshold for switching off the power supply is reached, the current is shut down with a dump time of few hundreds of milliseconds and the sample recovers the superconducting state.

In such case the temperature and voltage responses of the model are sensitive to the parameters that drive the Joule effect inside the interconnection. The tuning of the thermal and electrical resistances between the Cu stabilizer and the superconducting cables is therefore necessary, to take into account the contact resistances in addition to the SnAg bulk heat and current transport properties. The ratio of the tuned thermal and electrical conductivity yields a value of 3.5, which agrees with the $\alpha$ coefficient included in the Wiedemann–Franz law in [22] to account for impure materials. The computed and experimental temperatures presented in Fig. 10 are in good agreement, except for the initial transient state of the *U* temperature sensor. The corresponding voltage traces reported in [21] show as well very good agreement for different transport currents.

## 5. Parametric analyses

This section reports the parametric studies performed to assess the impact of several parameters on the interconnection critical defect length, assuming both adiabatic and non-adiabatic conditions. We used the model described in Section 3, which is simplified with respect to the one mentioned in the previous section while maintaining the fundamental physics. The critical defect length leading to thermal runaway is determined as a function of the current decay time constant $\tau_{dump}$, *RRR* of the SC cable copper matrix, *RRR* of the bus bar stabilizer and spatial distribution of the defect. The major effect of the heat transfer coefficient in the bus bar and in the interconnection region is investigated.

### 5.1. Parametric studies in adiabatic conditions

The first sets of simulations were performed in adiabatic conditions, thus neglecting the last term at left hand side of Eq. (1) con-

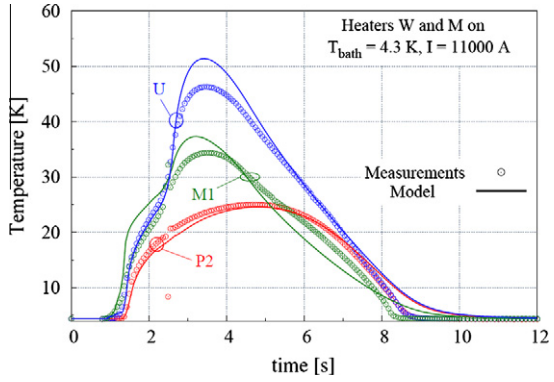


**Fig. 10.** Measured vs. calculated temperatures in case of 11 kA current and both heaters switched on.

cerning the heat exchange with helium. The temperature evolution as a function of time at different positions is shown in Fig. 11 for two defect lengths of the MB bus bar interconnection. Fig. 11 (left) and (right) refer to the case of a 7 and 8 mm long single defect, respectively. They constitute the maximum defect length allowing recovery and the minimum one leading to the interconnection burn out. The middle of the defect represents the hot spot, which in our calculations is located at the right extremity of the analyzed domain and corresponds to the longitudinal coordinate $x$ of 2 m. The temperature obviously decreases towards the bus bar inlet, but cannot decrease down to the initial temperature because adiabatic conditions were defined along the cable as well as at the boundaries. The longitudinal temperature gradient is located within 1 m from the defect, since the temperature profile is in practice the same at the coordinates 0.5 and 1 m.

After 15 s of almost uniform temperature rise all along the sample, the defect zone starts heating up faster than elsewhere. The larger Joule heating is due to the smaller available copper cross-section. The change of slope corresponds to that of the copper electrical resistivity vs. temperature. In case of Fig. 11 (left) the temperature remains always below 400 K. A recovery is observed because the rate of heat removal by conduction along the bus bar is greater than the rate of heat addition by the Joule effect. Therefore there is no further temperature increase. In case of Fig. 11 (right), in the same operating conditions but with a 1 mm longer defect, the behavior of the sample drastically changes. Although the situation is not different during the first 15 s, a thermal runaway occurs in the defect because the heat generated is not compensated anymore by the heat conduction mechanism. The hot spot temperature exceeds 500 K in about 25 s, which is referred to as burn out time. The sample integrity is not guaranteed any longer.

Based on these considerations, a curve can be traced reporting the minimum defect length leading to thermal runaway for different current levels, i.e. different beam energies. Such current will be referred to as limiting current, which leads to an interconnection hot spot temperature of 500 K. Two space regions are identified: a region of controlled quench corresponding to operating conditions located below this limiting current curve, and a region of thermal runaway above the curve. The difference between the largest defect leading to a controlled quench and the smallest defect leading to a thermal runaway is always of 1 mm, as in the case just mentioned. This difference is comparable to the uncertainty in the interconnection defect measurement in the LHC [4].

Fig. 12 reports the limiting current curves calculated for the MB (left) and MQ (right) interconnection in case of different current decay time constants $\tau_{dump}$: 50 and 100 s for MB; 10, 20 and 30 s for MQ. They correspond to the most probable $\tau_{dump}$ in case of a 3.5 and 7 TeV operation. Note that the same $\tau_{dump}$ is here assumed for any current/energy level. Although this is an approximation that does not reflect reality, it is useful to assess the influence of this parameter. The MQ interconnection exhibits a higher limiting current with respect to the MB one because of the shorter current decay time constant. The reduction of $\tau_{dump}$ allows significantly increasing the critical defect length in the whole current range. For MB it becomes between 20% and 50% larger when reducing $\tau_{dump}$ from 100 to 50 s, depending on the current. As for MQ, its increase is more relevant when reducing $\tau_{dump}$ from 20 to 10 s than from 30 to 20 s. $\tau_{dump}$ has such an impact on the critical defect length because it is comparable to the burn out time. A $\tau_{dump}$ much larger than the burn out time would feature a considerably smaller effect, as it will be the case in non-adiabatic conditions (Section 5.3). These results obtained in adiabatic conditions are in good agreement with other models [17], with differences within 10%.

As stated in Section 3.1, the defect length is directly proportional to $R_{add}$. The highest measured $R_{add}$ of 60 μΩ [16], which was repaired after the incident, is reported in Fig. 12 (left). This value is larger than the $R_{add}$ of 10 μΩ that should not be exceeded to allow operating the LHC at full energy. This is the reason for initially running the LHC at the limited energy of 3.5 TeV per beam with the current interconnection design, whereas a consolidation intervention is needed to reach the nominal beam energy of 7 TeV.

Fig. 13 presents the results obtained for different values of cable and bus bar copper Residual Resistivity Ratios (*RRR*s). The *RRR* is defined as the ratio of the copper resistivity at room temperature over its value at 10 K, which is just above the superconductor critical temperature $T_c$. The variation ranges were fixed according to measured values that were summarized in [17]: between 80 and 160 for $RRR_{cable}$ and between 100 and 220 for $RRR_{bus}$. For clarity, simulations carried out with the only boundary values are reported here. The effect of larger *RRR* values, permitting larger heat evacuation through longitudinal copper conduction, is only evident at small current levels. The cable copper has a larger impact than the bus bar copper. This is because the cable copper is in contact with the superconducting filaments, also inside the defect. For instance at 3500 A the $RRR_{cable}$ has a two to three times greater effect than the $RRR_{bus}$ on the critical defect length, when both are varied between the boundary values of their relative ranges.

So far the case of a single defect located on one side of the interconnection was considered. The defect can also be split in two parts, as shown in Fig. 14a. The additional resistance measurements performed throughout the whole interconnection do not allow distinguishing between single or double defect, which provide the same additional resistance $R_{add}$ in case of equal total length. The double defect case was analyzed according to the model shown in Fig. 14b, whose length is 4 m instead of 2. In order to obtain a direct comparison to the single defect case, in the following we will refer to the length of a double defect as the sum of its two parts. The investigated proportions between them are 50–50% and 75–25%.

Fig. 15 shows the temperature profiles along the 4 m long considered sample at different times. The double defect (50–50%) has a total length of 8 mm. A single defect of the same length in the same operating conditions leads to a thermal runaway, as it was shown in Fig. 11b. In this case instead, a recovery can be observed after a temperature rise up to ~200 K, where the peaks correspond to the middle points of the two defect parts. The split defect exhibits therefore higher limiting current with the same total length, thanks to larger longitudinal heat conduction from the hot spots.

Limiting current curves corresponding to double defects are presented in Fig. 16. The 50–50% case is reported, as well as the 75–25%. The latter has a smaller limiting current than the equally split defect because of the more severe conditions of its largest part. The splitting of the defect provides major increase of the crit-

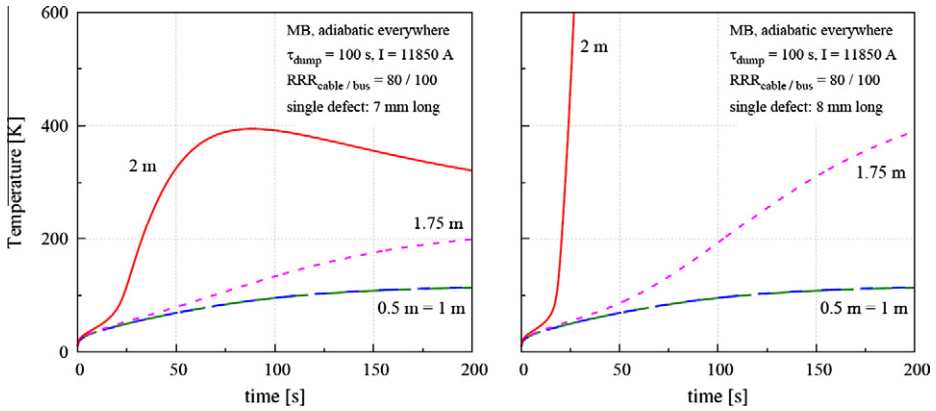


**Fig. 11.** Temperature evolution in time for a MB defect leading to a controlled quench (left) or to a thermal runaway (right), in adiabatic conditions.

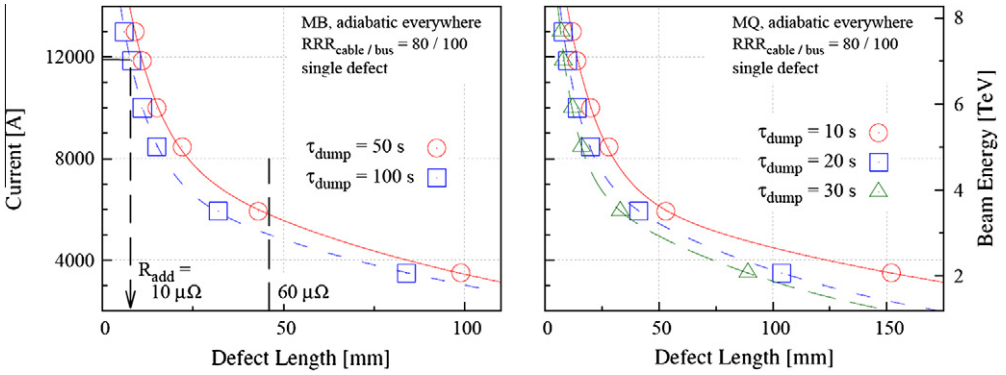


**Fig. 12.** Limiting current curve as a function of the current dump time for MB (left) and MQ (right) interconnection, in adiabatic conditions.

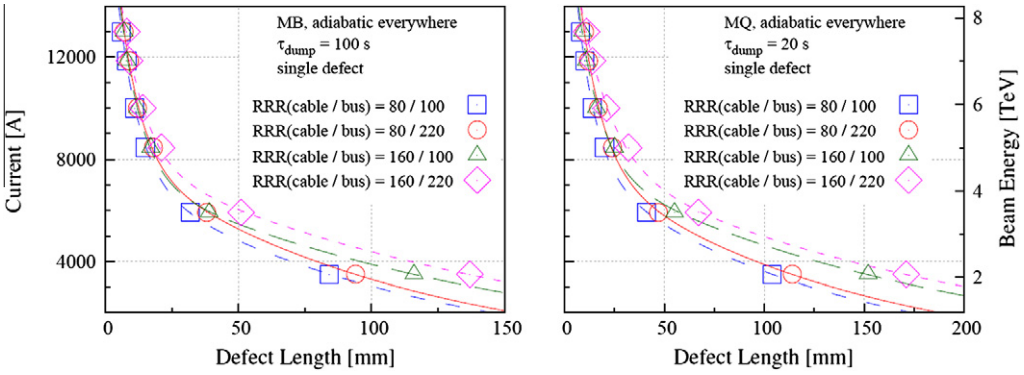


**Fig. 13.** Limiting current curve as a function of the cable and bus bar *RRR* for MB (left) and MQ (right) interconnection, in adiabatic conditions.

ical defect length at all current levels: it is of the order of 60% and 80% when going from a single defect (100–0%) to a 50–50% double one for the MB and MQ, respectively.

### 5.2. Impact of the heat transfer mechanisms

The previous results were obtained in the conservative hypothesis of adiabatic conditions. It is not the case of the LHC bus bars, which are immersed in a helium bath at 1.9 K. The present subsection analyzes the effects of helium cooling. Fig. 17 (left) reports the hot spot temperature evolution as a function of time for several defect lengths of the MB bus bar interconnection. With respect to the adiabatic case of Fig. 11, in the same operating conditions, the transverse heat transfer allows considerably increasing the critical defect length from 8 to 24 mm. The burn out time is consequently shorter, from 25 to 8 s, due to the larger associated heat generation that results from the increased $R_{add}$. As far as defects leading to controlled quench are concerned, larger defects feature higher peak temperatures and longer recovery times. A sudden temperature drop can be observed when the Joule heating is interrupted due to the resistive-to-superconducting transition of the whole sample. However, the transition does not occur at once: the discontinuity preceding the temperature drop corresponds indeed to the recovery of the region at the sample inlet.

Fig. 17 (right) summarizes the main features of simulations performed with various defect lengths: defects leading to controlled quench are characterized by the maximum hot spot temperature reached before recovery (left *y*-axis), whereas defects leading to thermal runaway are characterized by the burn out time (right *y*-axis). If the defect length is such that the hot spot temperature

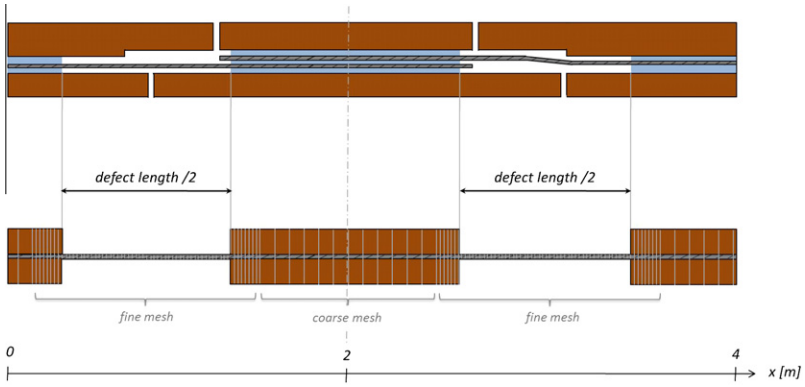


**Fig. 14.** Top: scheme of an interconnection with a double defect 50–50%. Bottom: model assumed for the calculations. Not to scale.

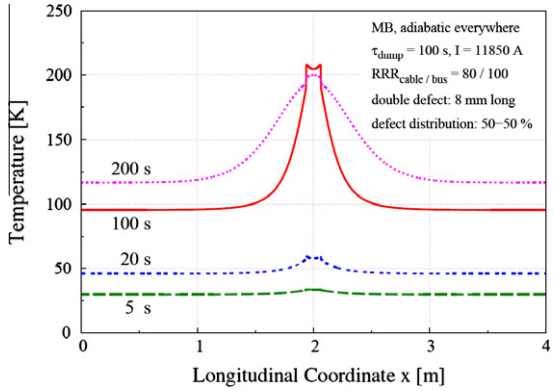


**Fig. 15.** Temperature profiles along the sample length for a MB double defect (50–50%) leading to a controlled quench, in adiabatic conditions.

exceeds ~35 K, the upper temperature limit is reached within 0.5–8 s. Because of the larger Joule heating, the burn out time decreases with increasing defect length. The vertical line dividing the two zones corresponds to the critical defect length. This last one will be the only information reported in the following figures.

The impact of the heat transfer on the interconnection limiting current is summarized in Fig. 18. As previously stated, the heat transfer mode in the interconnection region contains a residual uncertainty. Consequently, various hypotheses of cooling are made and compared to the fully adiabatic case representing the most pessimistic evaluation. We consider three cooling models, whose details can be found in Section 3.3 and in [19]:

- Adiabatic interconnection ($HTC_{ic} = 0$) and $HTC_{bus}$ to 1.9 K He II bath. This is considered the closest to reality, and can be seen as a reasonably conservative lower limit. It provides a double critical defect length with respect to the fully adiabatic case.
- $HTC_{bus}$ to 1.9 K He II bath, assumed to be the same over the whole sample length (i.e. $HTC_{ic} = HTC_{bus}$). This is an optimistic evaluation that allows increasing the critical defect length with respect to the fully adiabatic case by a factor 3.
- $HTC_{bus}$ to 4.25 K He I bath, assumed to be the same over the whole sample length (i.e. $HTC_{ic} = HTC_{bus}$). This case is reported for comparison. It features a smaller critical defect length with respect to the He II uniform cooling case, even though the corresponding HTC is larger (Fig. 6). This shows that the temperature difference between sample and bath has a larger impact than the HTC.

It can be concluded that the effect of heat transfer is substantial, and certainly predominant with respect to the other parameters.

### 5.3. Parametric studies in non-adiabatic conditions

Besides the assessment of the major improvement of the critical defect length due to helium cooling, we determined the effect of the parameters considered in Section 5.1 also in non-adiabatic conditions. The assumed cooling model is described by the $HTC_{bus}$ to 1.9 K He II bath assumed for the whole sample length.

The effect of the current decay time constant in non-adiabatic conditions is negligible, as shown in Fig. 19. This arises as under cooled conditions the critical defect length is larger, resulting in a higher $R_{add}$ and consequently faster burn out time. Considerable reduction of the MB current discharge time would be needed to produce a significant effect: $\tau_{dump}$ values below 10 s would be indeed comparable with the burn out time. The slight improvement observed for MQ is due to $\tau_{dump}$ values closer to the burn out time.

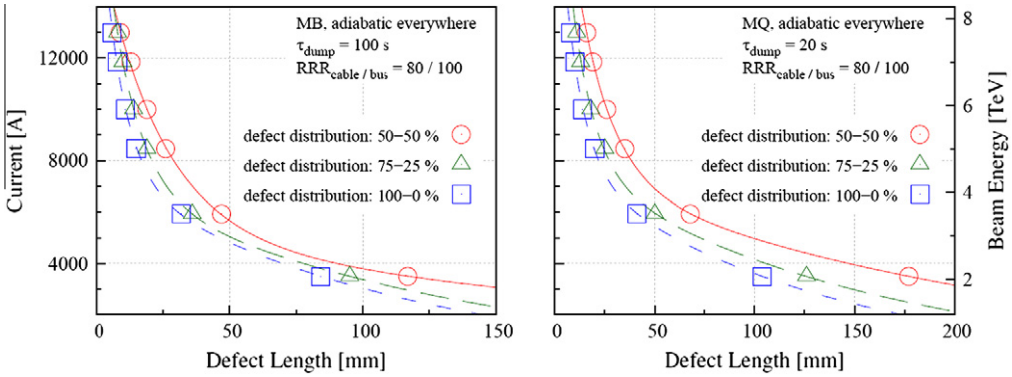


**Fig. 16.** Limiting current curve as a function of the defect spatial distribution for MB (left) and MQ (right) interconnection, in adiabatic conditions.

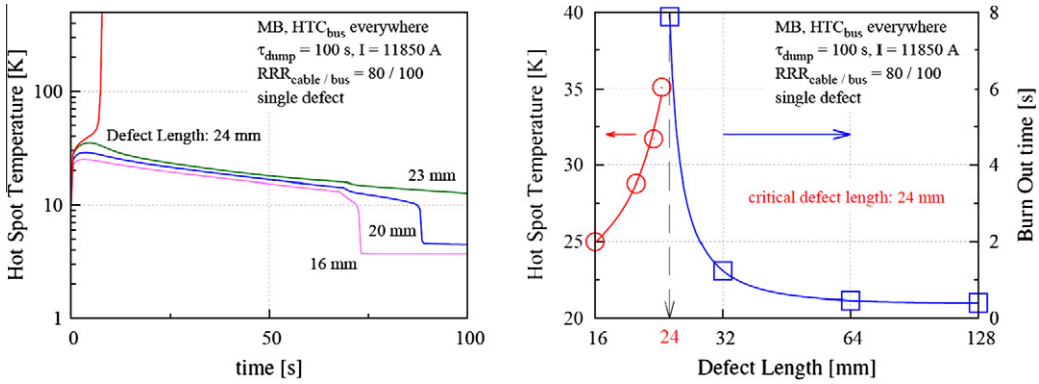


**Fig. 17.** Left: temperature evolution in time for different MB defects, in non-adiabatic conditions. Right: hot spot temperature for defects leading to controlled quench and burn out time for defects leading to thermal runaway.

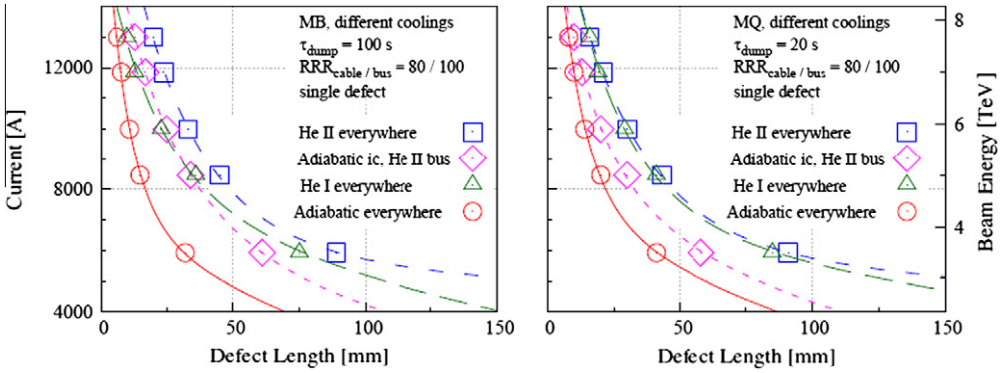


**Fig. 18.** Limiting current curve as a function of the cooling conditions for MB (left) and MQ (right) interconnection.

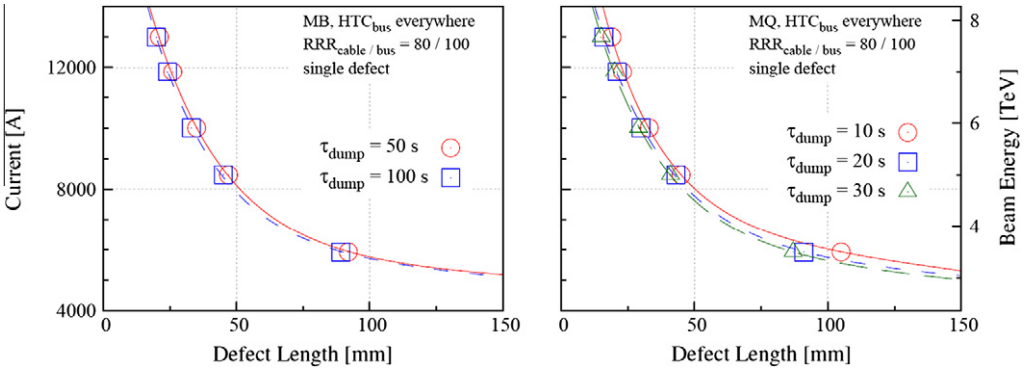


**Fig. 19.** Limiting current curve as a function of the current dump time for MB (left) and MQ (right) interconnection, in non-adiabatic conditions.

The helium cooling enhances the cable copper *RRR* effect, as shown in Fig. 20. The critical defect length roughly doubles when increasing $RRR_{cable}$ from 80 to 160. Such a behavior, although contradictory at a first glance, is due to the better heat conduction associated to a higher *RRR*. The heat generated in the hot spot spreads more easily in the longitudinal direction thus increasing the heat exchange surface to the bath. The effect is evident at all current levels. On the contrary the bus bar copper *RRR* has only a minor impact, as it was the case in adiabatic conditions.

As far as the splitting of the defect in cooled conditions is concerned, it permits a critical defect length improvement of the same order of magnitude as in the adiabatic case. Fig. 21 reports the relevant calculations.

## 6. Conclusions

A thermo-electric analysis of the bus bar interconnection of the LHC main dipole and quadrupole magnets was performed, following the 2008 incident, to estimate the critical length of potential interconnection manufacturing defects. A 1-D model was developed with particular care in the definition of transverse local heat transfer coefficients towards the cooling helium bath. Such approach was supported by dedicated measurements and analyses of heat transfer through the bus bar electrical insulation.

The model was validated by comparison to experimental tests of defective interconnections performed in He I bath. The calculations addressed the heat transfer coefficient through the intercon-

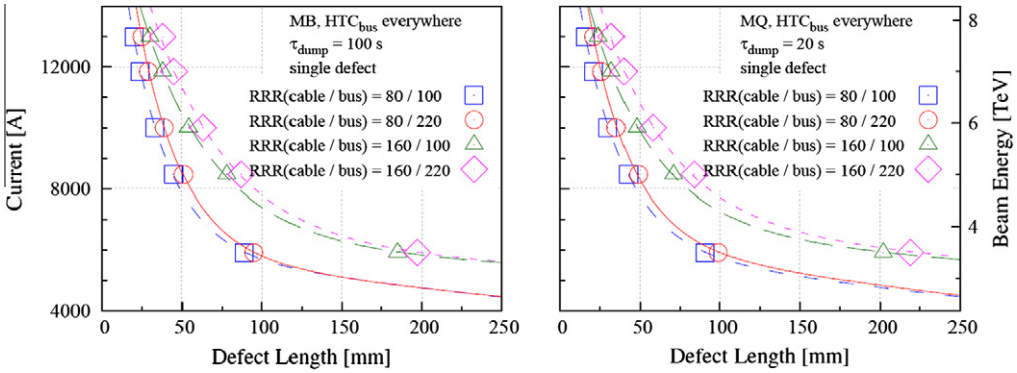


**Fig. 20.** Limiting current curve as a function of the cable and bus bar *RRR* for MB (left) and MQ (right) interconnection, in non-adiabatic conditions.

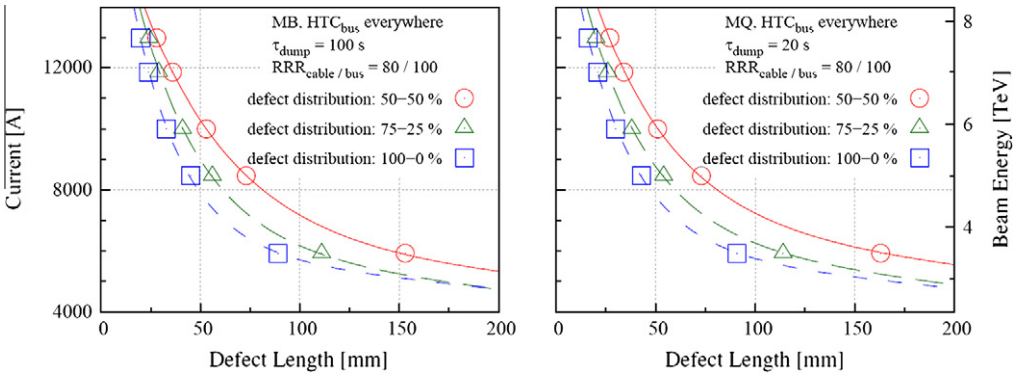


**Fig. 21.** Limiting current curve as a function of the defect spatial distribution for MB (left) and MQ (right) interconnection, in non-adiabatic conditions.

nection insulation, showing that the interconnection cannot be considered adiabatic. However, further investigations would be needed to completely describe the thermal mechanisms occurring in the interconnection. Therefore we made various hypothesis of cooling, which allowed identifying the predominant impact of the helium contribution on the limiting current, compared to the other parameters analyzed. The closest to reality assumption of He II cooled bus bar and adiabatic interconnection can be seen as a reasonably conservative lower limit. Such cooling model provides an increase of the critical defect length by a factor 2 with respect to the most pessimistic hypothesis of fully adiabatic conditions. The most optimistic hypothesis of He II bus bar heat transfer coefficient assumed for the whole sample length allows an increase by a factor 3.

The effect of parameters related to the interconnection manufacturing quality, operating conditions and protection system was estimated through sensitivity analyses. The cooling mode appears to strongly modify their influence on the limiting current. In particular:

- the impact of the current discharge time is significant in adiabatic conditions and negligible in non-adiabatic conditions. This is due to the different burn out time, comparable to the discharge time in the first case and much smaller in the second case.
- the cable *RRR* has a greater impact in cooled than in adiabatic conditions. The reason is the larger spread of heat in longitudinal direction, which increases the heat exchange surface to the bath. The bus bar *RRR* exhibits a low impact both in adiabatic and cooled case.
- the defect spatial distribution has a considerable effect both in adiabatic and non-adiabatic conditions.

The model complemented other evaluations used for the best estimates of interconnection critical additional resistances, preparing for LHC 2012 operation at the highest possible beam energies. Calculations were performed assuming the actual current dump time constants or possible longer values for beam energies between 3.5 and 4.5 TeV. The most pessimistic (adiabatic), most optimistic (full cooling) and most likely (partial cooling) conditions were considered, by varying cable/bus bar *RRR* and space distribution of the defect. These calculations showed that:

- MB and MQ limits obtained in adiabatic conditions, low cable/bus bar *RRR* (80/100), for single-sided defect are comparable to those quoted in previous analyses (e.g. $R_{add}$ = 43 μΩ for MB at 4 TeV, $\tau_{dump}$ of 52 s);
- an increase of the cable/bus bar *RRR* (160/220) to the values measured (bus) or expected (cable) in the LHC, and considering a soldering defect distributed in the interconnection (50–50%), yields an increase of the acceptable value of $R_{add}$ by more than a factor 2 ($R_{add}$ = 97 μΩ for MB at 4 TeV, $\tau_{dump}$ of 52 s);
- assuming conservative values for the cable/bus bar *RRR* (80/100) and single-sided defect, but considering realistic values for the heat transfer from bus bar to helium, yields a 50% increase of the acceptable value of $R_{add}$ ($R_{add}$ = 66 μΩ for MB at 4 TeV, $\tau_{dump}$ of 52 s).

## Acknowledgments

The authors wish to thank M. Bianchi who performed the simulations of the experimental tests during an internship at CERN. They are also grateful to F. Bertinelli, P. Fessia and D. Richter for the fruitful comments and suggestions, as well as to K. Dahlerup-

Petersen, A.P. Verweij and G.P. Willering for the useful information and data provided.

## References

[1] Rossi L. Superconductivity: its role, its success and its setbacks in the Large Hadron Collider of CERN. Supercond Sci Technol 2010;23.
[2] Baiko M et al. Report of the task force in the incident of 19th September 2008 at the LHC. CERN-LHC-PROJECT report-1168; 31 March, 2009.
[3] Koratzinos M et al. High-current bus splice resistances and implications for the operating energy of the LHC. In: Proceedings of IPAC'10, Kyoto, Japan; 2010. p. 373–5.
[4] Scheuerlein C et al. Production and quality assurance of main busbar splices during the LHC 2009 shutdown. IEEE Trans Appl Supercond 2011;21(3): 1786–90.
[5] Verweij AP et al. Consolidation of the 13 kA interconnects in the LHC for operation at 7 TeV. IEEE Trans Appl Supercond 2011;21(3):2376–9.
[6] The LHC design report CERN-2004-003, vol. 1. The LHC main ring, p. 157.
[7] Belova L, Genet M, Perinet-Marquet J-L, Ivanov P, Urpin C. Design and manufacture of the superconducting bus-bars for the LHC main magnets. IEEE Trans Appl Supercond 2002;12(1):1305–9.
[8] Dahlerup-Petersen K, Rodriguez-Mateos F, Schmidt R, Sonneman F. Energy extraction for the LHC superconducting circuits. CERN-LHC-PROJECT report-484; 2001.
[9] Jacquemod A, Poncet A, Schauf F, Skoczen B, Tock JPh. Inductive soldering of the junctions of the main superconducting busbars of the LHC. Presented at EUCAS, Sorrento, Italy; 2003.
[10] Laurent F, Tock JPh. Modification of the electrical insulation of main bus-bars interconnection. CERN LHC project document no. LHC-QQBID-EC-0001; 2009.
[11] Verweij AP. Busbar and joints stability and protection. In: Proceedings of Chamonix 2009 workshop on LHC performance; 2009, p. 110–116.
[12] Richter D. Private communication; 2009.
[13] Bottura L, Rosso C, Breschi M. A general model for thermal, hydraulic, and electric analysis of superconducting cables. Cryogenics 2000;40(8–10): 617–26.
[14] Breschi M, Granieri PP, Calvi M, Coccoli M, Bottura L. Quench propagation and stability analysis of Rutherford resistive core cables. Cryogenics 2006;46:606–14.
[15] Calvi M, Bottura L, Rodriguez Mateos F. Proposed method for the verification of the LHC bus bar splices during commissioning at cryogenic conditions. Presented at ASC, Seattle, USA; 2006.
[16] Bertinelli F et al. Towards a consolidation of LHC superconducting splices for 7 TeV operation, In: Proceedings of IPAC'10, Kyoto, Japan; 2010. p. 367–9.
[17] Verweij AP. Minimum requirements for the 13 kA splices for 7 TeV operation. In: Proceedings of Chamonix 2010 workshop on LHC performance; 2010. pp. 65–72.
[18] Le Coroller A, Deregel J, Henrichsen KN, Hervieu B, Juster FP, Perinet-Marquet J-L, et al. Measurement of superconducting busbars models for the LHC main dipole. IEEE Trans Appl Supercond 2000;10(1):1118–21.
[19] Granieri PP, Casali M, Richter D. Heat transfer in the LHC main superconducting bus bars. In: Proceedings of ICEC 23 – ICMC 2010, Wroclaw, Poland; 2010. pp. 411–6.
[20] Willering GP, Bottura L, Fessia P, Scheuerlein C, Verweij AP. Thermal runaways in LHC interconnections: experiments. IEEE Trans Appl Supercond 2011;21(3):1781–5.
[21] Granieri PP, Casali M, Bianchi M, Breschi M, Bottura L, Willering GP. Analysis of defective interconnections of the 13 kA LHC superconducting bus bars. IEEE Trans Appl Supercond 2012;22(3):400054.
[22] Lei Y, Yu Y, Dai Y, Nan H. Measurements of the interstrand thermal and electrical conductance in multistrand superconducting cables. IEEE Trans Appl Supercond 2002;12(1):1052–5.